

Polarization manipulation of bright-dark vector bisolitons

Yan Zhou(周延), Xiaoyan Lin(林晓艳), Meisong Liao(廖梅松), Guoying Zhao(赵国营), and Yongzheng Fang(房永征)

Citation: Chin. Phys. B, 2021, 30 (**3**): 034208. DOI: 10.1088/1674-1056/abd76d
Journal homepage: http://cpb.iphy.ac.cn; http://iopscience.iop.org/cpb

What follows is a list of articles you may be interested in

Efficient manipulation of terahertz waves by multi-bit coding metasurfaces and further applications of such metasurfaces

Yunping Qi(祁云平) Baohe Zhang(张宝和), Jinghui Ding(丁京徽), Ting Zhang(张婷), Xiangxian Wang(王向贤), and Zao Yi(易早)

Chin. Phys. B, 2021, 30 (**2**): 024211. DOI: 10.1088/1674-1056/abd6fc

Polarization-independent silicon photonic grating coupler for large spatial light spots

Lijun Yang(杨丽君), Xiaoyan Hu(胡小燕), Bin Li(李斌), and Jing Cao(曹静)

Chin. Phys. B, 2021, 30 (**2**): 024206. DOI: 10.1088/1674-1056/abbc00

Broadband asymmetric transmission for linearly and circularly polarization based on sand-clock structured metamaterial

Tao Fu(傅涛), Xing-Xing Liu(刘兴兴), Guo-Hua Wen(文国华), Tang-You Sun(孙堂友), Gong-Li Xiao(肖功利), and Hai-Ou Li(李海鸥)

Chin. Phys. B, 2021, 30 (**1**): 014201. DOI: 10.1088/1674-1056/abb662

Multi-functional vanadium dioxide integrated metamaterial for terahertz wave manipulation

Jian-Xing Zhao(赵建行), Jian-Lin Song(宋建林), Yao Zhou(周姚), Rui-Long Zhao(赵瑞龙), Yi-Chao Liu(刘艺超), Jian-Hong Zhou(周见红)

Chin. Phys. B, 2020, 29 (**9**): 094205. DOI: 10.1088/1674-1056/abab6f

Pulse shaping of bright-dark vector soliton pair

Yan Zhou(周延), Yuefeng Li(李月锋), Xia Li(李夏), Meisong Liao(廖梅松), Jingshan Hou(侯京山), Yongzheng Fang(房永征)

Chin. Phys. B, 2020, 29 (**5**): 054202. DOI: 10.1088/1674-1056/ab7b56

Polarization manipulation of bright-dark vector bisolitons*

Yan Zhou(周延)[1], Xiaoyan Lin(林晓艳)[1], Meisong Liao(廖梅松)[2,†], Guoying Zhao(赵国营)[3], and Yongzheng Fang(房永征)[3,‡]

[1] School of Science, Shanghai Institute of Technology, Shanghai 201418, China
[2] Key Laboratory of Materials for High Power Laser, Shanghai Institute of Optics and Fine Mechanics, Chinese Academy of Sciences, Shanghai 201800, China
[3] School of Materials Science and Engineering, Shanghai Institute of Technology, Shanghai 201418, China

(Received 6 December 2020; revised manuscript received 27 December 2020; accepted manuscript online 30 December 2020)

We simulate the polarization manipulation of bright-dark vector bisolitons at 1-μm wavelength regime. Through changing the pulse parameters, different kinds of pulse shapes and optical spectra are generated in output orthogonal polarization directions. When the input vector bisoliton is polarization-locked with 1064 nm central wavelength, "1+1" fundamental dark-dark and "2+1" pseudo-high-order bright-dark group-velocity-locked vector solitons can be achieved through changing the projection angle. When the input vector bisoliton is group-velocity-locked with 1063 nm and 1065 nm central wavelengths, "2+1" and "2+2" pseudo-high-order bright-dark group-velocity-locked vector solitons, bright-dark group-velocity-locked vector solitons with chirp-like temporal oscillations are generated. Our simulation results can provide beneficial conduct for polarization manipulation of vector multi-solitons, and have promising applications in quantum information register, optical communications, nanophotonics, and all-optical switching.

Keywords: polarization manipulation, vector bisoliton, polarization-locking, group-velocity-locking, linear birefringence

PACS: 42.25.Ja, 42.25.Lc, 42.55.Wd, 42.65.–k **DOI:** 10.1088/1674-1056/abd76d

1. Introduction

Optical solitons have potential applications in the fields of optical communications and optical information processing.[1–3] Passively mode-locked ultrafast fiber laser is often constructed to study soliton dynamics.[4–7] More often, vector soliton can be generated in fiber laser because the intrinsic linear birefringence of the single-mode fiber, which is brought by strain, temperature variation, and fabrication imperfection. In theory, the vector soliton in a dissipative fiber laser system can be well described using coupled Ginzburg–Landau equations, which include fiber dispersion, gain, loss, self-phase modulation, cross-phase modulation, coherent energy coupling, gain bandwidth, and so on.[1,6] In experiment, different kinds of vector solitons can be generated through changing intra-cavity linear birefringence and pump power, such as group-velocity-locked vector soliton (GVLVS),[9–11] polarization-locked vector soliton (PLVS),[12,13] and polarization rotation vector soliton (PRVS).[14] For GVLVS, the two orthogonal polarization modes will shift their central wavelengths in opposite directions and copropagate as a unit without splitting. PLVS has fixed polarization state ($\pm\pi/2$ phase difference in orthogonal polarization directions) and orthogonal polarization modes have the same central wavelength. PRVS has fixed soliton intensity accompanied with periodically evolving polarization state, and the evolving period is multiple of intra-cavity pulse transmission period.

Vector solitons with different pulse shapes properties have also been reported, such as bright-bright vector soliton, bright-dark vector soliton, and dark-dark vector soliton. Among them, the bright-dark vector soliton has one pulse peak in one polarization direction and one dip in the orthogonal polarization direction. It can exist in normal or anomalous dispersion regime, which is different from its scalar counterpart.[15,16]

Until now, there have been many reports about vector solitons at different wavelengths. Out-cavity polarization manipulation of vector solitons has also been reported. For example, Jin *et al.* theoretically and experimentally demonstrated the manipulation of GVLVS in an Er-doped passively mode-locked fiber laser system, and finally generated "2+1" and "2+2" type pseudo-high-order GVLVSs.[17,18] Wang *et al.* numerically analyzed the decomposition and recombination of group-velocity-locked vector dissipative solitons.[19] Zhu *et al.* experimentally showed the generation of high-order vector soliton structure based on group-velocity-locked vector dissipative solitons.[20] In our previous work, we theoretically simulated the polarization manipulation of PLVS with super-Gaussian pulses,[21] dark-dark vector solitons,[22] bright-dark vector solitons,[16] parabolic vector solitons,[23] and vector bisolitons[24] at 1-μm wavelength regime. However, there are few reports about polarization manipulation of bright-dark vector bisolitons. In this work, we theoretically simulate the polarization manipulation of polarization- and group-velocity-locked bright-dark vector bisolitons in a polarization-resolved

*Project supported by National Key Research and Development Program of China (Grant No. 2018YFB0504500), the National Natural Science Foundation of China (Grant No. 51672177), and Shanghai Sailing Program (Grant No. 20YF1447500).

†Corresponding author. E-mail: liaomeisong@siom.ac.cn
‡Corresponding author. E-mail: fangyongzheng@sit.edu.cn

© 2021 Chinese Physical Society and IOP Publishing Ltd

fiber system at 1-μm wavelength regime. It is found that different kinds of pulse shapes and corresponding optical spectra can be generated through changing the pulse parameters of the orthogonal polarization modes. Our simulation results can provide beneficial evidence for the study of manipulating vector multi-solitons.

2. Theoretical model and simulation

Figure 1 shows the theoretical model in our simulation. Input vector bisoliton with amplitudes of A_1 and A_2 in vertical and horizontal directions suffers from amplitude ratio (A_2/A_1) change, time delay (ΔT) change, and linear birefringence (Δn) change one by one. At last, the modulated vector bisoliton is collimated by the collimator (Col) and incident on the polarization beam splitter (PBS). The two orthogonal electric fields are separated by the PBS in orthogonal transmission directions. In experiment, A_2/A_1 can be changed by a fiber amplifier or fiber attenuator, ΔT can be tuned with a fiber time delay line, Δn is changed by rotating the polarization controller (PC), and projection angle θ is achieved through rotating PBS.

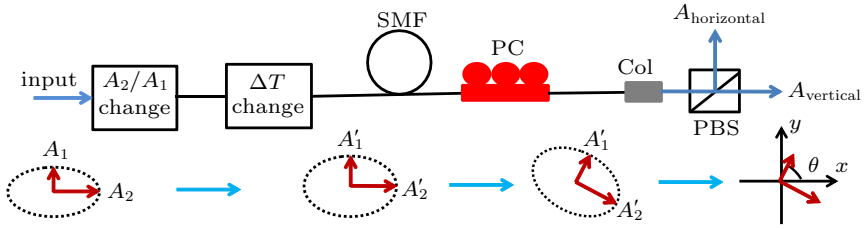


Fig. 1. Theoretical model in the simulation.

The electric fields before the PBS can be written as

$$A_1'(t) = A_1\left\{\operatorname{sech}\left[\frac{1.763(t-\Delta T/2-T_{\text{interval}}/2)}{T_1}\right] + \operatorname{sech}\left[\frac{1.763(t-\Delta T/2+T_{\text{interval}}/2)}{T_1}\right]\right\} \times \mathrm{e}^{\mathrm{i}\frac{2\pi ct}{\lambda_1}}, \quad (1)$$

$$A_2'(t) = A_2\left\{\tanh\left[\frac{1.763(t+\Delta T/2-T_{\text{interval}}/2)}{T_2}\right] + \tanh\left[\frac{1.763(t+\Delta T/2+T_{\text{interval}}/2)}{T_2}\right]\right\} \times \mathrm{e}^{\mathrm{i}\left(\frac{2\pi ct}{\lambda_2}+\Delta\varphi\right)}, \quad (2)$$

where $A_1'(t)$ and $A_2'(t)$ are the bright and dark electric fields of vertical mode and horizontal mode before the PBS; A_1 and A_2 are the maximum amplitudes; T_1 and T_2 are the pulse widths; λ_1 and λ_1 are the central wavelengths; and ΔT and $\Delta\varphi$ are the time delay and phase difference between the orthogonal modes. $\Delta\varphi$ includes two parts: one is the intrinsic linear birefringence of the input vector bisoliton, the other is the externally imposed linear birefringence brought through rotating PC. It should be mentioned that $\Delta\varphi$ can be precisely controlled by changing the rotation angle of the three paddles of PC. c is the light velocity in vaccum, t is the time parameter, and T_{interval} is the time separation between the bright or dark bisolitons.

After the PBS, the projected horizontal mode $A_{\text{horizontal}}$ and vertical mode A_{vertical} are

$$A_{\text{horizontal}} = A_1'(t)\cos\theta + A_2'(t)\sin\theta, \quad (3)$$

$$A_{\text{vertical}} = A_1'(t)\sin\theta - A_2'(t)\cos\theta. \quad (4)$$

In later simulations, we assume $T_1 = T_2 = 5$ ps, $T_{\text{interval}} =$ 20 ps. It should be noted that here we do not consider dispersion and nonlinearity in the single-mode fiber in our model, because we assume that the fiber length is much shorter compared with the dispersion length and nonlinearity length. The fiber dispersion length can be increased through reducing the net group-velocity dispersion (with fixed pulse width), while the fiber nonlinear length can be increased by decreasing the pulse peak power. Of course, we can replace the piece of single-mode fiber and the imposed PC by several waveplates to change the linear birefringence, but it will broke the all-fiber structure.

2.1. With the same central wavelength

In this section, we consider the vector bisoliton with the same central wavelength $\lambda_1 = \lambda_2 = 1064$ nm, which can be generated in the Yb-doped passively mode-locked vector bisoliton fiber laser. In the first three cases, $\Delta\varphi$ is fixed at $\pi/2$ because it is the characteristic of PLVS. In the last case, $\Delta\varphi$ is varied from 0 to π through gradually rotating the PC.

Firstly, the amplitude ratio is changed for simulation. Figure 2 gives the simulated temporal pulse shapes and corresponding optical spectra when amplitude ratio A_2/A_1 is 1/1.5, 1/1.2, 1/1, 1.2/1, and 1.5/1 respectively. While the other parameters are $\theta = 0°$, $\Delta T = 0$ ps, and $\Delta\varphi = \pi/2$. In Figs. 2(a)–2(e), we can see that as A_2/A_1 increases, there are always two pulse peaks in the horizontal direction and only one broad dip in the vertical direction. Also, the dip depth has an obvious increase when A_2/A_1 reaches 1.2/1. In the corresponding optical spectra shown in Figs. 2(f)–2(j), both orthogonal polarization modes have only one peak, and the peak intensity of the vertical mode is always higher than that of the horizontal mode, although the amplitude ratio is smaller than 1.

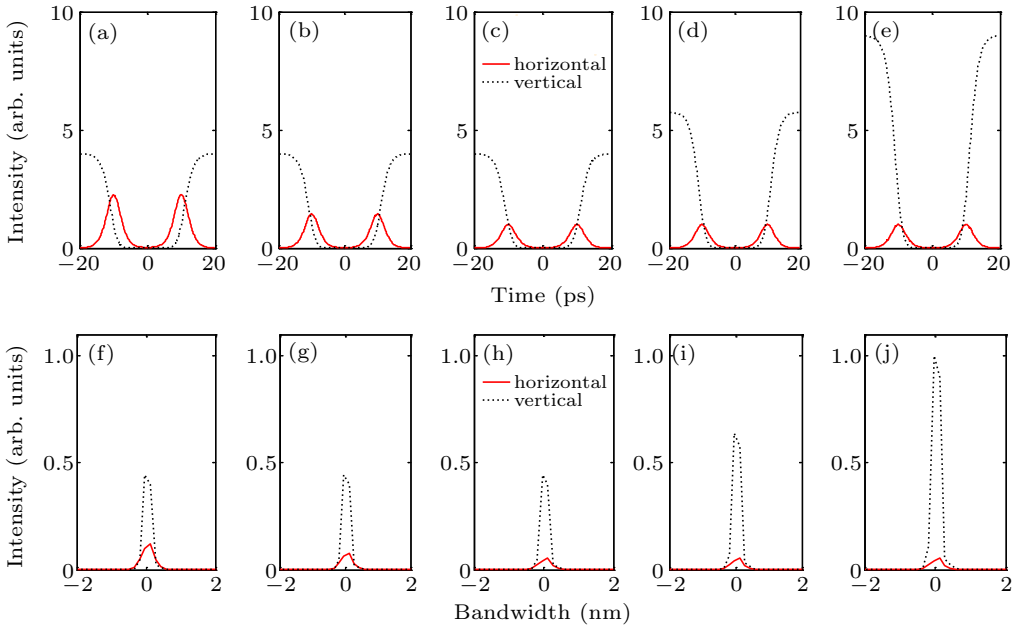


Fig. 2. Modulated temporal pulse shapes (a)–(e) and corresponding optical spectra (f)–(j) in horizontal and vertical polarization directions when the amplitude ratio is changed.

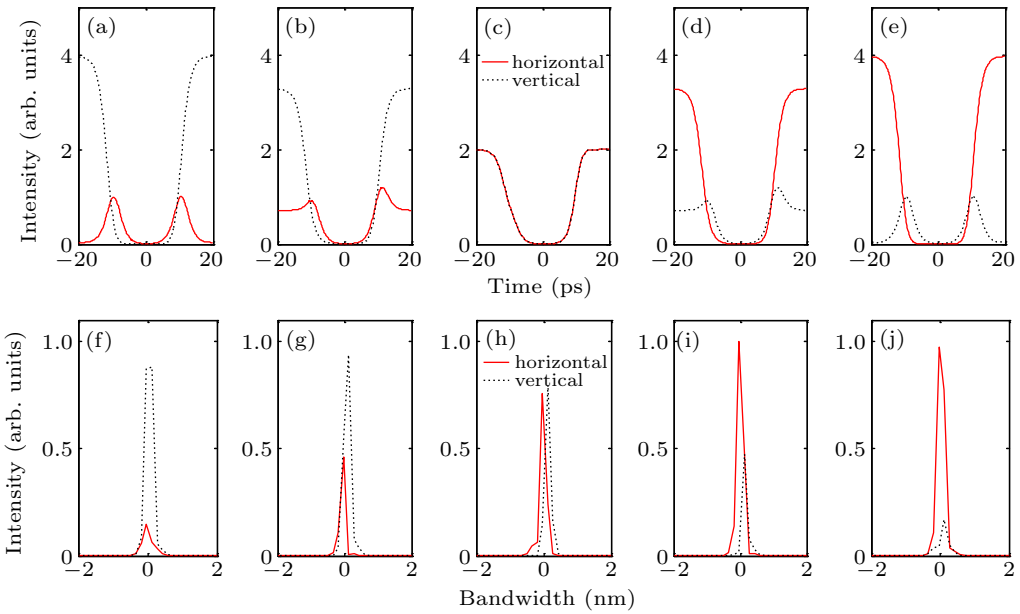


Fig. 3. Modulated temporal pulse shapes (a)–(e) and corresponding optical spectra (f)–(j) in horizontal and vertical polarization directions when the projection angle is changed.

Then, the projection angle is varied for simulation. Figure 3 gives the simulated temporal pulse shapes and corresponding optical spectra when θ is 5°, 25°, 45°, 65°, and 85° respectively. The other parameters are $A_2/A_1 = 1/1$, $\Delta T = 1$ ps, and $\Delta\varphi = \pi/2$. In Figs. 3(a)–3(e), there are two peaks in the horizontal/vertical mode and one dip in the vertical/horizontal mode when θ is smaller/larger than 45°. And there is only one broad dip for the orthogonal polarization modes and they are coincide with each other when $\theta = 45°$ under symmetry projection. In the corresponding optical spectra shown in Figs. 3(f)–3(j), the central wavelengths of the orthogonal polarization modes are slightly different. The horizontal/vertical mode has blue/red shift accompanied with peak intensity variation, which may be due to the energy transfer between the two orthogonal modes. So "1+1" fundamental dark-dark and "2+1" pseudo-high-order bright-dark GVLVSs can be generated through changing θ. The difference between high-order vector soliton and pseudo-high-order vector soliton is that the phases in the orthogonal polarization directions are locked/unlocked for the high-order vector soliton/pseudo-high-order vector soliton.

After that, the time delay change is considered in simulation. Figure 4 shows the temporal pulse shapes in the orthogonal polarization directions when the time delay is increased from 2 ps to 20 ps with 2 ps time interval. The other parameters are $A_2/A_1 = 1/1$, $\theta = 43°$, and $\Delta\varphi = \pi/2$. We can see

that there is only one broad dip in the orthogonal polarization directions when $\Delta T = 2$ ps, and another dip will appear when ΔT reaches 4 ps. The dip depths of these two dips become equal when $\Delta T = 10$ ps. Besides, there is a new pulse peak at the position of continuous wave background when ΔT starts with 2 ps, and the peak intensity of the vertical mode is always higher than that of the horizontal mode. The two orthogonal modes have similar pulse shapes near peak/dip position but with obvious different continuous wave backgrounds. In the corresponding optical spectra demonstrated in Fig. 5, the optical spectrum splits for the orthogonal polarization modes when ΔT increases from 2 ps to 14 ps, and there are side peaks when ΔT is larger than 14 ps. The maximum peak intensity of the horizontal mode decreases with increased time delay. While for the vertical mode, the maximum peak intensity is relatively steady with increased time delay.

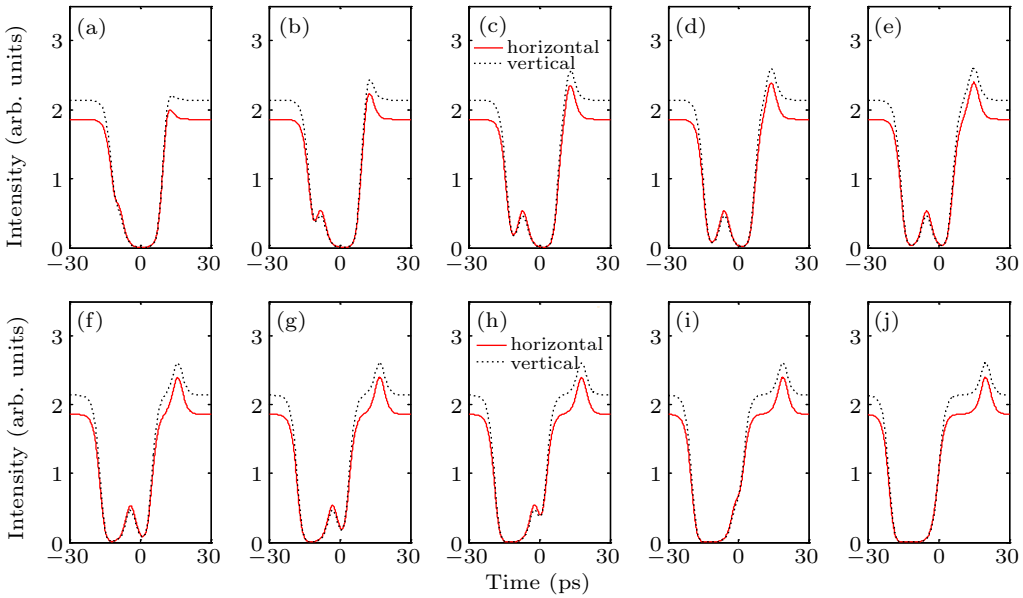


Fig. 4. Modulated temporal pulse shapes in horizontal and vertical polarization directions when the time delay is changed.

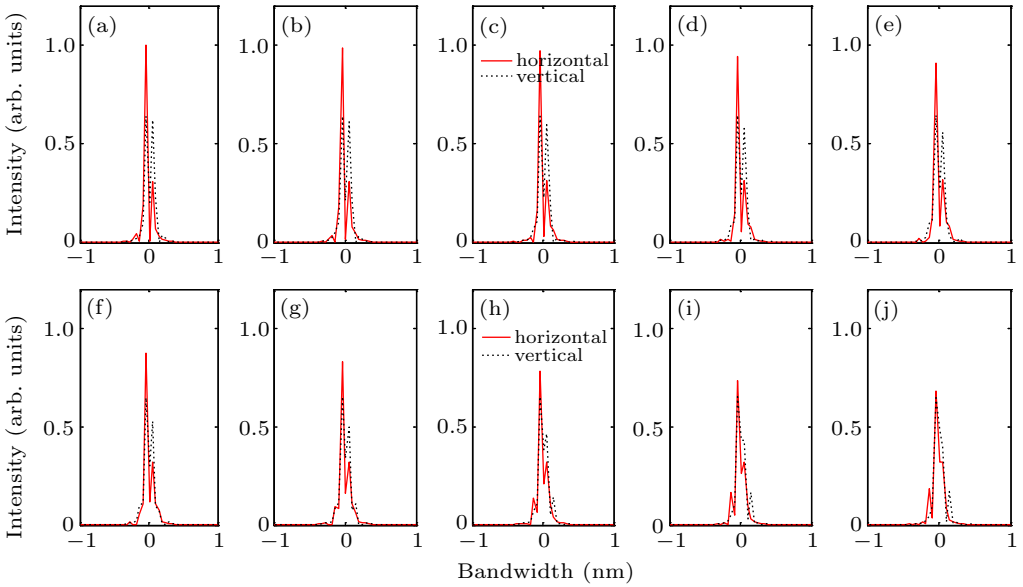


Fig. 5. Optical spectra corresponding to Fig. 4.

At last, we consider the case when the phase difference is 0, $\pi/4$, $\pi/2$, $3\pi/4$, and π, and the simulation results are shown in Fig. 6. The other parameters are $A_2/A_1 = 1/1$, $\theta = 45°$, and $\Delta T = 0$ ps. We can see that the optical spectra of the orthogonal modes are coincide with each other but the pulse shapes are not when $\Delta\varphi$ is 0 or π. While the pulse shapes of the orthogonal modes are coincide with each other but the optical spectra are not (with different central wavelengths and different peak intensities) when $\Delta\varphi$ is $\pi/2$. There is only one dip for the orthogonal modes when $\Delta\varphi$ is $\pi/4$, $\pi/2$, or $3\pi/4$, and two dips when $\Delta\varphi$ is 0 or $\pi/2$. Besides, another peak appears when $\Delta\varphi$ is not equal to $\pi/2$.

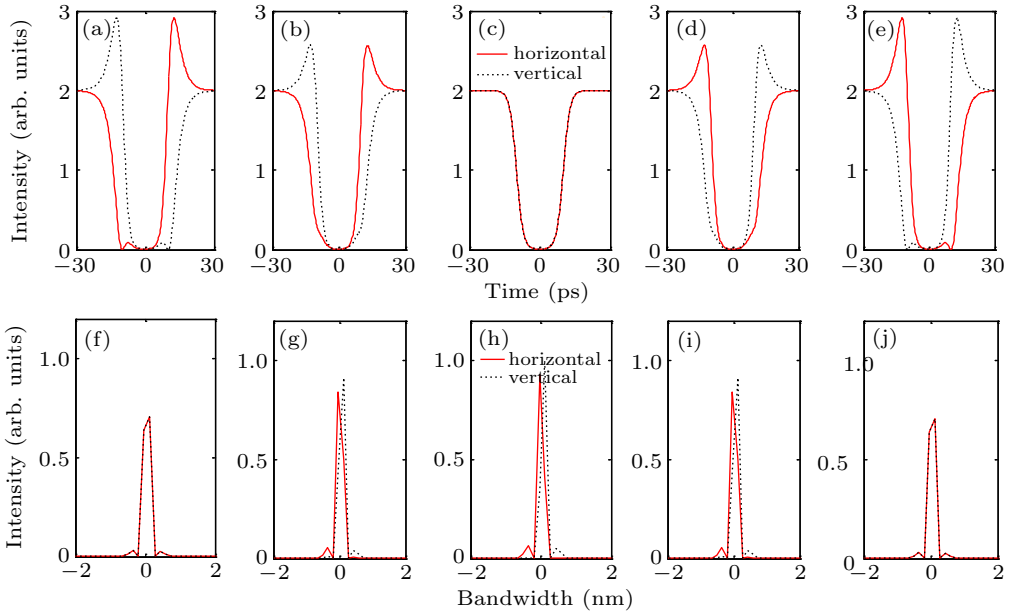


Fig. 6. Modulated temporal pulse shapes (a)–(e) and corresponding optical spectra (f)–(j) in horizontal and vertical polarization directions when the phase difference is changed.

2.2. With different central wavelengths

In this section, we simulate the polarization manipulation of bright-dark vector bisoliton with different central wavelengths ($\lambda_1 = 1063$ nm, $\lambda_2 = 1065$ nm), and it is the characteristic of GVLVS. Because GVLVS has unfixed phase difference, in the first three cases we assume $\Delta\varphi = 0$ for simplicity. In the last case, $\Delta\varphi$ is varied from 0 to π through gradually rotating the PC.

Similar to Subsection 2.1, firstly we simulate the output pulse shapes and optical spectra when the amplitude ratio is changed. Figure 7 gives the simulated temporal pulse shapes and corresponding optical spectra when amplitude ratio A_2/A_1 is 1/1.5, 1/1.2, 1/1, 1.2/1, and 1.5/1 respectively. While the other parameters are $\theta = 0°$, $\Delta T = 0$ ps, and $\Delta\varphi = 0$. We can see that as the amplitude ratio increases, the horizontal mode and vertical mode always have two peaks and two dips, respectively. In the corresponding optical spectra shown in Figs. 7(f)–7(j), both orthogonal modes have only one peak and the peak intensity of the vertical mode is always higher than that of the horizontal mode regardless of the amplitude ratio. So "2+2" pseudo-high-order bright-dark GVLVS is generated in this situation.

Then, we consider the case of changing projection angle. Figure 8 gives the simulated temporal pulse shapes and corresponding optical spectra when θ is 5°, 25°, 45°, 65°, and 85° respectively. The other parameters are $A_2/A_1 = 1/1$,

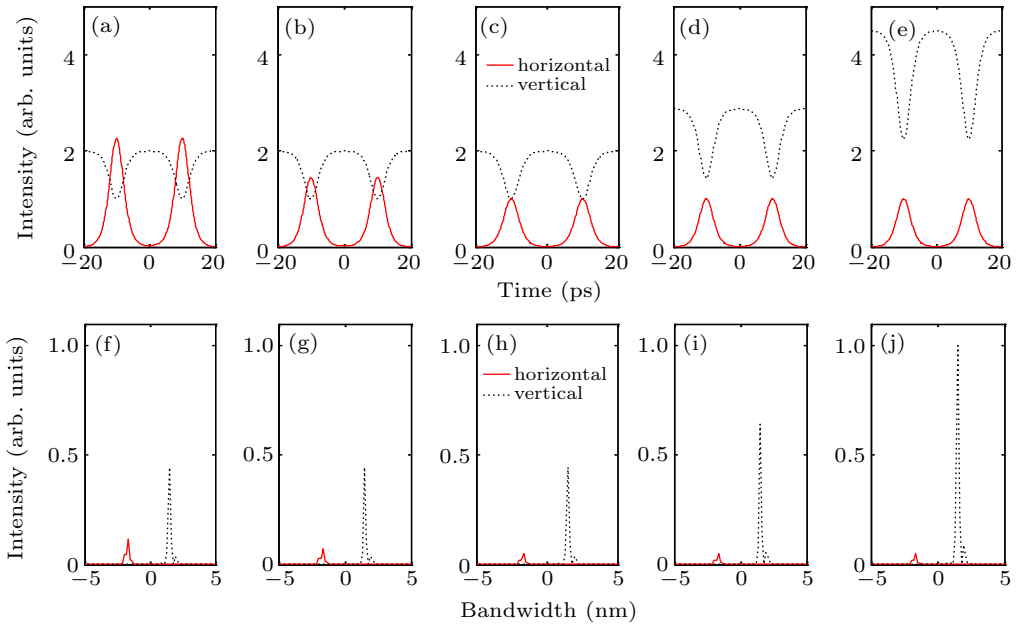


Fig. 7. Modulated temporal pulse shapes (a)–(e) and corresponding optical spectra (f)–(j) in horizontal and vertical polarization directions when the amplitude ratio is changed.

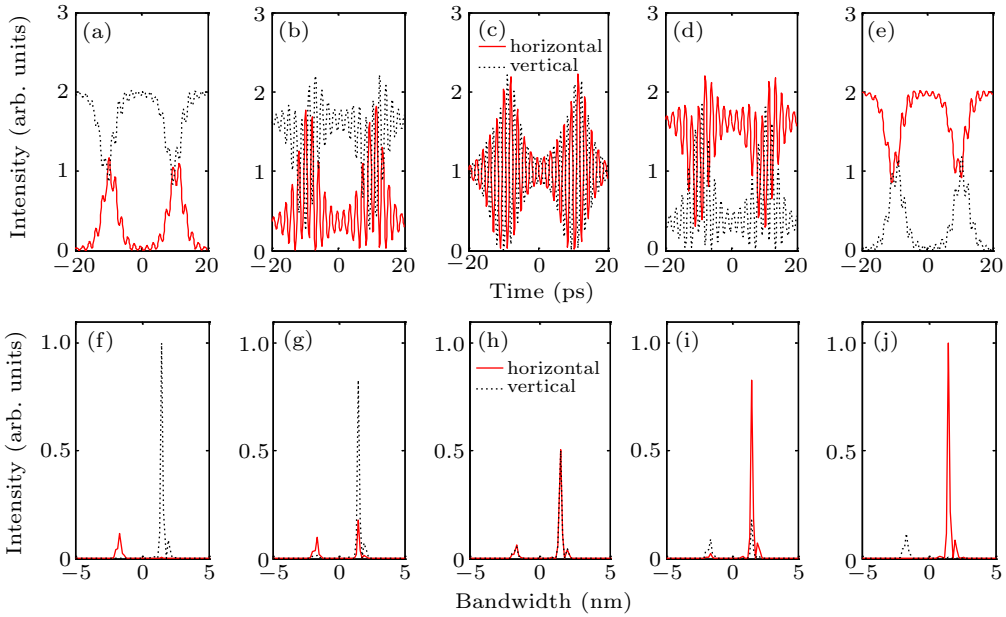


Fig. 8. Modulated temporal pulse shapes (a)–(e) and corresponding optical spectra (f)–(j) in horizontal and vertical polarization directions when the projection angle is changed.

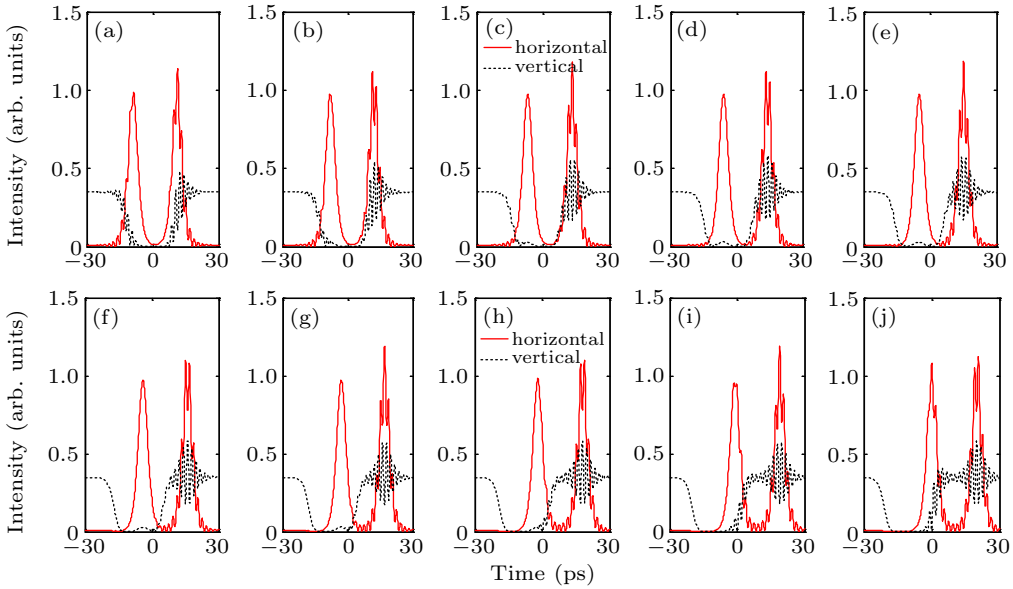


Fig. 9. Modulated temporal pulse shapes in horizontal and vertical polarization directions when the time delay is changed.

$\Delta T = 1$ ps, and $\Delta\varphi = 0$. The horizontal/vertical mode has multiple side peaks/dips when θ is 5°, and the result becomes contrary for the orthogonal polarization modes when θ is 85°. And the peak/dip oscillation will become higher when θ is approaching 45°. The temporal pulse oscilloscopes of the orthogonal modes will become the same when θ is 45°. In the optical spectra shown in Figs. 8(f)–8(j), the peak intensity of longer wavelength is always higher than that of shorter wavelength, and there are two peaks in the horizontal/vertical mode when θ is 25°/65°. In this case, most energy is concentrated at longer wavelength although $A_2/A_1 = 1/1$.

After that, we simulate the output pulse shapes and optical spectra when the time delay changes from 2 ps to 20 ps with 2 ps time interval. The other parameters are $A_2/A_1 = 0.3/1$, $\theta = 10°$, and $\Delta\varphi = 0$. Figures 9 and 10 show the simulation results. In Fig. 9, for the horizontal mode, there are two pulse peaks, and the lagged pulse has obvious temporal oscillations across the entire pulse. While for the vertical mode, there is only one broad pulse dip, and the trailing pulse edge has chirp-like oscillations. The broad pulse dip has slight split when ΔT changes from 6 ps to 14 ps. The time interval of the orthogonal modes increases with increased ΔT. Figure 10 demonstrates the optical spectra corresponding to Fig. 9. It shows that with the increase of ΔT, there is always one peak located at shorter/longer wavelength position for the horizontal/vertical mode, and there is another peak with much smaller peak intensity located at longer/shorter wavelength position for the horizontal/vertical mode. The main peak intensity of

the vertical mode is much higher than that of the horizontal mode, and the peak intensity of the orthogonal modes has a slight decrease with increased ΔT.

At last, we simulate the temporal pulse shapes and corresponding optical spectra when $\Delta\varphi$ is 0, $\pi/4$, $\pi/2$, $3\pi/4$, and π respectively. The other parameters are $A_2/A_1 = 0.3/1$, $\theta = 1°$, and $\Delta T = 0$ ps. Figure 11 shows the simulation results. We can see that the smooth temporal pulse shapes and optical spectra do not have obvious changes when $\Delta\varphi$ is changed, which means that the output "2+1" pseudo-high-order bright-dark GVLVS is insensitive to the change of phase difference. In the optical spectra shown in Figs. 11(f)–11(j), the horizontal mode is located at 1061 nm and there are two side peaks. While the vertical mode is located at 1067 nm with one sharp peak, and the peak intensity of the vertical mode is always higher than that of the horizontal mode although the input amplitude ratio is 0.3.

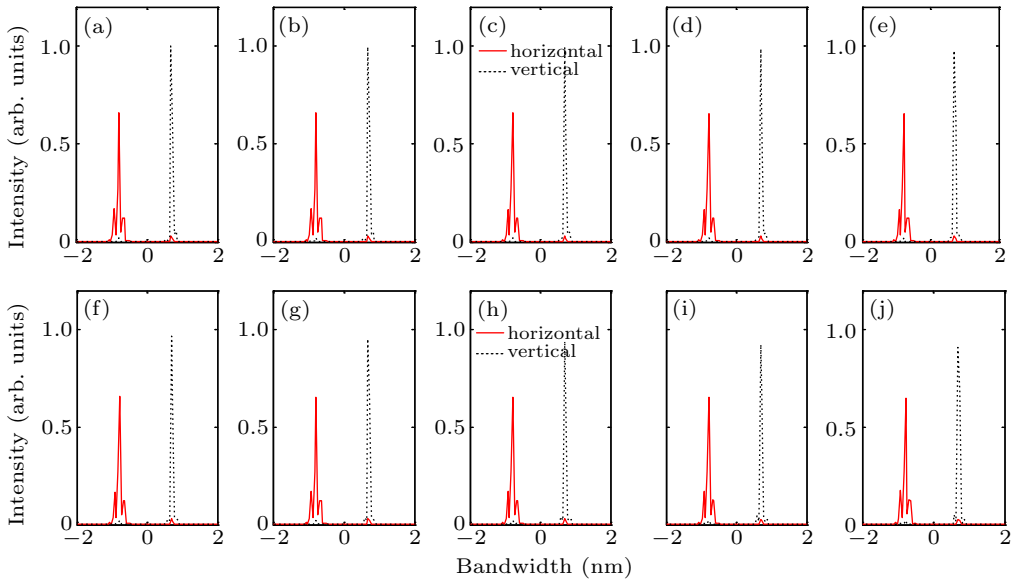


Fig. 10. Optical spectra corresponding to Fig. 9.

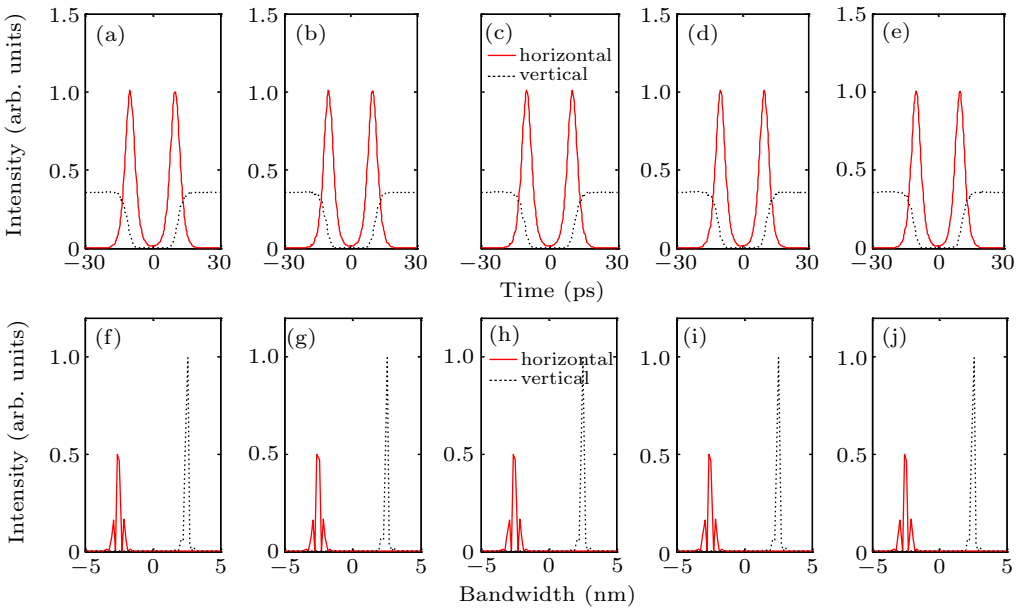


Fig. 11. Modulated temporal pulse shapes (a)–(e) and optical spectra (f)–(j) in horizontal and vertical polarization directions when the phase difference is changed.

3. Conclusion

We simulated the polarization manipulation of 1-μm polarization- and group-velocity-locked bright-dark vector bisolitons in a polarization resolved optical fiber system. In the simulation, through changing the amplitude ratio, projection angle, time delay, and phase difference of the orthogonal polarization modes, different kinds of vector solitons were generated in orthogonal polarization directions, such as "1+1" fundamental dark-dark GVLVS, PLVS with two dips and one peak in orthogonal polarization directions, "2+1" and "2+2"

pseudo-high-order bright-dark GVLVSs. Also, GVLVSs with multiple temporal oscillations could be generated with appropriate pulse parameters. Our simulation can provide beneficial conduct for manipulation of vector multi-solitons.

References

[1] Zhang P, Hu C, Zhou Q, Biswas A and Liu W J 2020 *Nonlinear Dyn.* **101** 1215

[2] Wang H B, Han H N, Zhang Z Y, Shao X D, Zhu J F and Wei Z Y 2020 *Chin. Phys. B* **29** 030601

[3] Song Y F, Shi X J, Wu C F, Tang D Y and Zhang H 2019 *Appl. Phys. Rev.* **6** 021313

[4] Liu X M, Yao X K and Cui Y D 2018 *Phys. Rev. Lett.* **121** 023905

[5] Liu X M and Pang M 2019 *Laser Photonics Rev.* **13** 1800333

[6] Liu X M, Popa D and Akhmediev N 2019 *Phys. Rev. Lett.* **123** 093901

[7] Dou Z Y, Zhang B, Cai J H and Hou J 2020 *Chin. Phys. B* **29** 094201

[8] Wang L L and Liu W J 2020 *Chin. Phys. B* **29** 070502

[9] Menyuk C R 1987 *Opt. Lett.* **12** 614

[10] Luo Y Y, Xiang Y, Shum P P, Liu Y S, Xia R, Ni W J, Lam H Q, Sun Q Z and Tang X H 2020 *Opt. Express* **28** 4216

[11] Hu X, Guo J, Shao G D, Song Y F, Yoo S W, Malomed B A and Tang D Y 2019 *Opt. Express* **27** 18311

[12] Cundiff S T, Collings B C, Akhmediev N N, Soto-Crespo J M, Bergman K and Knox W H 1999 *Phys. Rev. Lett.* **82** 3988

[13] Hu X, Guo J, Shao G D, Song Y F, Zhao L M, Li L and Tang D Y 2020 *Phys. Rev. A* **101** 063807

[14] Li T J, Liu M, Luo A P, Luo Z C and Xu W C 2020 *Opt. Express* **28** 32010

[15] Ma J, Shao G D, Song Y F, Zhao L M, Xiang Y J, Shen D Y, Richardson M and Tang D Y 2019 *Opt. Lett.* **44** 2185

[16] Zhou Y, Li Y F, Li X, Liao M S, Hou J S and Fang Y Z 2020 *Chin. Phys. B* **29** 054202

[17] Jin X X, Wu Z C, Zhang Q, Li L, Tang D Y, Shen D Y, Fu S N, Liu D M and Zhao L M 2015 *IEEE Photon. J.* **7** 7102206

[18] Jin X X, Wu Z C, Li L, Zhang Q, Tang D Y, Shen D Y, Fu S N, Liu D M and Zhao L M 2016 *IEEE Photon. J.* **8** 1501206

[19] Wang X, Li L, Geng Y, Wang H X, Su L and Zhao L M 2018 *Appl. Opt.* **57** 746

[20] Zhu S N, Wu Z C, Fu S N and Zhao L M 2018 *Appl. Opt.* **57** 2064

[21] Zhou Y, Li Y F, Zhang R L, Wang T X, Bi W J, Li X, Kuan P W, Fang Y Z and Liao M S 2019 *Optik* **194** 163132

[22] Zhou Y, Li Y F, Li X, Zhao G Y, Hou J S, Zou J, Fang Y Z and Liao M S 2020 *Optik* **203** 163925

[23] Zhou Y, Li Y F, Li Y G, Li X, Zhao G Y, Liao M S and Fang Y Z 2020 *Optik* **224** 165699

[24] Zhou Y, Li X, Zhao G Y, Liao M S and Fang Y Z 2021 *Optik* **227** 166022